AIAA JOURNAL
Vol. 40, No. 2, February 2002

Wall-Normal-Free Reynolds-Stress Model for Rotating Flows Applied to Turbomachinery

G. A. Gerolymos* and I. Vallet†
Université Pierre-et-Marie-Curie, 91405 Orsay, Paris, France

A recently developed near-wall wall-normal-free Reynolds stress model is extended and applied to the computation of transonic three-dimensional flows in turbomachinery rotors with tip clearance. The Reynolds stress model used is completely independent of the distance-from-the-wall and of the normal-to-the-wall direction. This is achieved by using a pseudonormal direction, defined by the gradients of turbulence length scale and anisotropy tensor invariants, in the pressure–strain echo terms. The effects of rotation are included through the exact Coriolis terms in the Reynolds stress transport equations and through the isotropization of absolute flow-production model used for the rapid pressure–strain terms. The model is initially validated by comparison with measurements in rotating fully developed plane channel flows. Computational results obtained with the proposed Reynolds stress model are compared with measurements and with k–ε computations for various operating points of the NASA 37 rotor, using a 3×10^6 multiblock computational grid with 41 radial stations within the tip-clearance gap. The proposed model substantially improves the agreement with measurements compared to existing algebraic and two-equation models.

Introduction

DESPITE the important advances of steady[1–10] and unsteady[11–17] turbomachinery computational fluid dynamics (CFD), the predictive capability of the complex turbulent flows encountered in turbomachinery aerodynamics[18–28] can be substantially enhanced by improved turbulence modeling.[29–33] Following the pioneering work of Hah[34,35] and Hah et al.,[36] the current state of the art in turbulence models used for turbomachinery CFD has evolved toward the systematic use of two-equation closures,[37–54] such as k–ε (Refs. 55–57), k–ω_T (Refs. 58 and 59), k–ℓ_T (Ref. 60), k–τ_T (Ref. 61) or k–ζ_T (Ref. 62), including near-wall low-turbulence Reynolds number terms that make these models independent of wall topology. The integration up to the wall is extremely important in complex geometries because, to quote Bradshaw,[33] "matching to wall functions is not trivial, and programming and running time may be reduced by integrating a fixed-up (low-turbulence Reynolds number) model to the wall." Using two-equation models is a definite advantage compared to mixing-length or one-equation models,[63,64] because, as remarked by Ekaterinaris and Menter,[65] the "ambiguity of defining the length scale," especially in the wake or the tip-clearance regions,[7,8] is avoided.

Numerous variants of two-equation models have been developed over the years,[66–70] differing mainly in the scale-determining equation (for ε, ω_T, ℓ_T, τ_T, or ζ_T). All of these models are, however, based on the Boussinesq hypothesis of tensorial proportionality between the mean-rate-of-deformation and the Reynolds stresses (see Refs. 29–33). For complex three-dimensional flows with large separation[50] and intense mixing[19] (both of which are characteristic of turbomachinery), the Boussinesq hypothesis can be a serious drawback (see Ref. 27). When considering flows within turbomachinery rotors, the inability of predicting the effects of rotation on turbulence and as a consequence on secondary flow mixing is added to the previous problems.[29] It is well established that the effects of streamline curvature[71] and of system rotation[72] on the mean flow are produced through modification of turbulence structure (or more specifically of the Reynolds stress tensor anisotropy). For this reason anisotropic models are necessary. Under this general label are included full Reynolds stress transport models[73] (RSM), algebraic Reynolds-stress models[29,74] (ARSM) and nonlinear two-equation closures,[60] also called explicit ARSM (EARSM).[75] Although taking into account the spectral energy transfer, through the use of multiscale models,[76–81] is of course important, this technique should be used in conjuction with anisotropic models.

Numerous EARSM models have been proposed with variable degrees of success.[82–89] The usual justification for not using the full RSM closure is that it is much more expensive[88] and less stable.[89] The increasing number of studies[90–96] using full RSM closures for complex separated flows suggests that it is possible to overcome these drawbacks. The authors[97] have developed a wall-normal-free near-wall RSM closure that has given results systematically better than two-equation models and has proven to be extremely robust thanks to a carefull implementation of realizability constraints.[98] With the particular implicit implementation used (Gerolymos, G. A., and Vallet, I., manuscript in preparation) the RSM computations are only 30% more time consuming than a conventional low Reynolds k–ε model.

The purpose of this paper is to extend the near-wall RSM closure developed by Gerolymos and Vallet[97] to rotating flows and to apply it to transonic turbomachinery flows with tip clearance. The proposed closure is completely independent of the distance-from-the-wall and of the normal-to-the-wall direction. The resulting turbulence transport equations are field equations requiring the knowledge of local flow values only. This makes the use of the model in complex geometries with multiblock grids straightforward. The model performance is assessed by comparison with experimental data 1) for fully developed plane channel flow subjected to spanwise rotation[72] and 2) for three-dimensional flow in a transonic compressor rotor.[22,99]

Wall-Normal-Free RSM

Mean Flow

The flow is modeled by the compressible Favre–Reynolds averaged three-dimensional Navier–Stokes equations,[47,97] written in a reference frame rotating with rotational velocity $\boldsymbol{\Omega} = \Omega_i \boldsymbol{e}_i$,

$$\frac{\partial \bar{\rho}}{\partial t} + \frac{\partial \bar{\rho} \tilde{W}_\ell}{\partial x_\ell} = 0 \tag{1}$$

$$\frac{\partial \bar{\rho} \tilde{W}_i}{\partial t} + \frac{\partial}{\partial x_\ell}[\bar{\rho} \tilde{W}_i \tilde{W}_\ell + \bar{p}\delta_{i\ell}] + 2\bar{\rho}\epsilon_{ij\ell}\Omega_j \tilde{W}_\ell + \bar{\rho}\frac{\partial}{\partial x_i}\left[-\frac{1}{2}\Omega^2 R^2\right] - \frac{\partial}{\partial x_\ell}[\bar{\tau}_{i\ell} - \bar{\rho}\widetilde{w_i'' w_\ell''}] = 0 \tag{2}$$

Received 9 September 2000; revision received 20 July 2001; accepted for publication 13 August 2001.

*Professor, Director, Laboratoire d'Energétique, Unité Associée au Centre National de Recherche Scientifique, Bâtiment 511.

†Assistant Professor, Laboratoire d'Energétique, Unité Associée au Centre National de Recherche Scientifique, Bâtiment 511.

$$\frac{\partial}{\partial t}\left[\bar{\rho}\breve{h}_{t_W}-\bar{p}\right]+\frac{\partial}{\partial x_\ell}\left[\bar{\rho}\tilde{W}_\ell\left(\breve{h}_{t_W}-\frac{1}{2}\Omega^2R^2\right)\right]$$

$$-\frac{\partial}{\partial x_\ell}[\tilde{W}_i(\bar{\tau}_{i\ell}-\bar{\rho}\widetilde{w_i''w_\ell''})-(\bar{q}_\ell+\bar{\rho}\widetilde{h''w_\ell''})]=S_{\breve{h}_t} \tag{3}$$

where t is the time, x_ℓ the Cartesian space coordinates in the relative frame of reference, ϵ_{ijk} the third-order antisymmetric tensor,[100] δ_{ij} the Kronecker symbol,[100] R the radius (distance from the axis of rotation, $R^2=[x_i-|\Omega|^{-2}x_j\Omega_j\Omega_i][x_i-|\Omega|^{-2}x_j\Omega_j\Omega_i]$), W_i the relative velocity components, $V_i=W_i+\epsilon_{ijk}\Omega_jx_k$ the absolute velocity components, ρ the density, p the pressure, and τ_{ij} the viscous stresses. The tilde indicates Favre averaging, the over bar nonweighted averaging, the double prime Favre fluctuations, and the single prime nonweighted-fluctuations. Here, $\breve{h}_{t_W}=\tilde{h}+\frac{1}{2}\tilde{W}_i\tilde{W}_i$ is the total enthalpy of the relative mean flow (which is different from the Favre averaged total enthalpy $\tilde{h}_{t_W}=\tilde{h}+\frac{1}{2}\tilde{W}_i\tilde{W}_i+k=\breve{h}_{t_W}+k$), where h is the specific enthalpy, $k=\frac{1}{2}\widetilde{w_i''w_i''}$ is the turbulence kinetic energy, and w_i'' is the frame-independent velocity fluctuations. The symbol ($\breve{}$) is used to denote a function of average quantities that is neither a Favre average nor a nonweighted average. The source term in the mean energy equation is [93,97]

$$S_{\breve{h}_t}=-\left(P_k-\bar{\rho}\varepsilon+\overline{p'\frac{\partial w_\ell''}{\partial x_\ell}}\right)+\frac{\partial}{\partial x_\ell}[\overline{pw_\ell''}]+(-\bar{p}\delta_{i\ell}+\bar{\tau}_{i\ell})\frac{\partial\overline{w_i''}}{\partial x_\ell} \tag{4}$$

where $P_k=\frac{1}{2}P_{\ell\ell}$ is the turbulence kinetic energy production (equal to one-half of the trace of the Reynolds stresses production tensor P_{ij}) and ε is its dissipation.

Thermodynamics and Basic Closures

The thermodynamics of the working gas are approximated by[101]

$$\bar{p}=\bar{\rho}R_g\tilde{T}=\bar{\rho}\frac{\gamma-1}{\gamma}\tilde{h}$$

$$\breve{\mu}=\mu(\tilde{T})=\mu_{273}\frac{\tilde{T}^{\frac{3}{2}}}{273.15^{\frac{3}{2}}}\frac{T_S+273.15}{T_S+\tilde{T}}$$

$$\breve{\kappa}=\kappa(\tilde{T})=\kappa_{273}\frac{\mu(\tilde{T})}{\mu_{273}}[1+A_\kappa(\tilde{T}-273.15)] \tag{5}$$

where γ is the isentropic exponent, R_g the gas constant, μ the dynamic viscosity, and κ the heat conductivity. For air $R_g=287.04\ \mathrm{m^2\cdot s^{-2}\cdot K^{-1}}$, $\gamma=1.4$, $\mu_{273}=17.11\times10^{-6}\ \mathrm{Pa\cdot s}$, $\kappa_{273}=0.0242\ \mathrm{W\cdot m^{-1}\cdot K^{-1}}$, $T_S=110.4\ \mathrm{K}$, and $A_\kappa=0.00023\ \mathrm{K^{-1}}$. The mean viscous stresses are approximated in the usual way by[102,103]

$$\bar{\tau}_{ij}\cong\breve{\mu}\left(\frac{\partial\tilde{W}_i}{\partial x_j}+\frac{\partial\tilde{W}_j}{\partial x_i}-\frac{2}{3}\frac{\partial\tilde{W}_\ell}{\partial x_\ell}\delta_{ij}\right),\qquad \bar{q}_i\cong-\breve{\kappa}\frac{\partial\tilde{T}}{\partial x_i} \tag{6}$$

In the present work the turbulent heat-flux $\bar{\rho}\widetilde{h''w_i''}$ is closed by a simple gradient model[102]

$$\bar{\rho}\widetilde{h''w_i''}=-\frac{\mu_Tc_p}{Pr_T}\frac{\partial\tilde{T}}{\partial x_i},\qquad c_p=\frac{\gamma}{\gamma-1}R_g,\qquad \mu_T=C_\mu\breve{\mu}Re_T^*$$

$$C_\mu=0.09\exp\left[-\frac{3.4}{\left(1+0.02Re_T^*\right)^2}\right],\qquad Re_T^*=\frac{\bar{\rho}k^2}{\breve{\mu}\varepsilon^*} \tag{7}$$

where c_p is the heat capacity at constant pressure, Pr_T the turbulent Prandtl number (in the present work, $Pr_T=0.9$ to obtain the correct recovery temperature for turbulent flow over an adiabatic wall), and Re_T^* the turbulence Reynolds number based on the modified dissipation[55] $\varepsilon^*=\varepsilon-2\breve{\nu}(\mathrm{grad}\sqrt{k})^2$ (ε being turbulence kinetic energy dissipation and $\breve{\nu}$ the kinematic viscosity).

Reynolds Stress Transport

The transport equations for the Favre–Reynolds averaged Reynolds stresses, written in the relative (rotating) frame-of-reference and taking into account the density fluctuations effects, are[29,104]

$$\underbrace{\frac{\partial\bar{\rho}\widetilde{w_i''w_j''}}{\partial t}+\frac{\partial}{\partial x_\ell}(\bar{\rho}\widetilde{w_i''w_j''}\tilde{W}_\ell)}_{\text{convection } C_{ij}}$$

$$=\underbrace{\frac{\partial}{\partial x_\ell}(-\bar{\rho}\widetilde{w_i''w_j''w_\ell''}-\overline{p'w_j''}\delta_{i\ell}-\overline{p'w_i''}\delta_{j\ell}+\overline{w_i''\tau_{j\ell}'+w_j''\tau_{i\ell}'})}_{\text{diffusion } d_{ij}}$$

$$+\underbrace{\overline{p'\left(\frac{\partial w_i''}{\partial x_j}+\frac{\partial w_j''}{\partial x_i}-\frac{2}{3}\frac{\partial w_k''}{\partial x_k}\delta_{ij}\right)}}_{\text{redistribution } \phi_{ij}}$$

$$+\underbrace{(-2\bar{\rho}\epsilon_{i\ell m}\Omega_\ell\widetilde{w_j''w_m''}-2\bar{\rho}\epsilon_{j\ell m}\Omega_\ell\widetilde{w_i''w_m''})}_{\text{Coriolis redistribution } G_{ij}}$$

$$+\underbrace{\left(-\bar{\rho}\widetilde{w_i''w_\ell''}\frac{\partial\tilde{W}_j}{\partial x_\ell}-\bar{\rho}\widetilde{w_j''w_\ell''}\frac{\partial\tilde{W}_i}{\partial x_\ell}\right)}_{\text{production } P_{ij}}$$

$$-\underbrace{\overline{\left(\tau_{j\ell}'\frac{\partial w_i''}{\partial x_\ell}+\tau_{i\ell}'\frac{\partial w_j''}{\partial x_\ell}\right)}}_{\text{dissipation } \bar{\rho}\varepsilon_{ij}}+\underbrace{\frac{2}{3}\overline{p'\frac{\partial w_k''}{\partial x_k}}\delta_{ij}}_{\text{pressure–dilatation}}$$

$$+\underbrace{\left(-\overline{w_i''}\frac{\partial\bar{p}}{\partial x_j}-\overline{w_j''}\frac{\partial\bar{p}}{\partial x_i}+\overline{w_i''}\frac{\partial\bar{\tau}_{j\ell}}{\partial x_\ell}+\overline{w_j''}\frac{\partial\bar{\tau}_{i\ell}}{\partial x_\ell}\right)}_{\text{density fluctuation effects } K_{ij}} \tag{8}$$

Convection C_{ij} and production P_{ij} are exact terms. The modeling concerning the remaining terms is discussed in the following section.

Compressibility, Diffusion, and Dissipation

In the present model[97] direct compressibility effects K_{ij}, pressure–dilatation correlation, and pressure–diffusion are neglected:

$$K_{ij}\cong0,\qquad \overline{p'\frac{\partial w_\ell''}{\partial x_\ell}}\cong0,\qquad \overline{pw_\ell''}\cong0$$

$$\overline{w_i''}\cong0,\qquad S_{\breve{h}_t}\cong-(P_k-\rho\varepsilon) \tag{9}$$

Because pressure–diffusion is neglected, diffusion is approximated by

$$d_{ij}\cong\frac{\partial}{\partial x_k}\left[-\bar{\rho}\widetilde{w_i''w_j''w_k''}+\breve{\mu}\frac{\partial\widetilde{w_i''w_j''}}{\partial x_k}\right] \tag{10}$$

where the triple correlations are modeled following Hanjalić and Launder,[105]

$$\widetilde{w_i''w_j''w_k''}\cong-C_s\frac{k}{\varepsilon}$$

$$\times\left[\widetilde{w_i''w_\ell''}\frac{\partial\widetilde{w_j''w_k''}}{\partial x_\ell}+\widetilde{w_j''w_\ell''}\frac{\partial\widetilde{w_k''w_i''}}{\partial x_\ell}+\widetilde{w_k''w_\ell''}\frac{\partial\widetilde{w_i''w_j''}}{\partial x_\ell}\right]$$

$$C_s=0.11 \tag{11}$$

A transport equation for the modified dissipation rate (for which the wall boundary-condition is $\varepsilon_w^*=0$)

$$\varepsilon^*=\varepsilon-2\breve{\nu}\left(\mathrm{grad}\sqrt{k}\right)^2,\qquad \bar{\rho}\breve{\nu}=\breve{\mu} \tag{12}$$

is used, based on the Launder–Sharma[57] equation, but with a tensorial diffusion coefficient.[93,97] The modeled form of the equation is[93,106]

$$\frac{\partial \bar{\rho}\varepsilon^*}{\partial t} + \frac{\partial}{\partial x_\ell}\left(\tilde{W}_\ell \bar{\rho}\varepsilon^*\right) - \frac{\partial}{\partial x_\ell}\left[\left(\breve{\mu}\delta_{k\ell} + C_\varepsilon \frac{k}{\varepsilon^*}\bar{\rho}\widetilde{w_k'' w_\ell''}\right)\frac{\partial \varepsilon^*}{\partial x_k}\right]$$

$$= C_{\varepsilon 1} P_k \frac{\varepsilon^*}{k} - C_{\varepsilon 2}\bar{\rho}\frac{\varepsilon^{*2}}{k} + \frac{2\breve{\mu}\mu_T}{\bar{\rho}}(\nabla^2 \tilde{\boldsymbol{W}})^2 \tag{13}$$

$$C_\varepsilon = 0.18, \qquad C_{\varepsilon 1} = 1.44, \qquad C_{\varepsilon 2} = 1.92\left(1 - 0.3e^{-Re_T^{*2}}\right) \tag{14}$$

Pressure–Strain Redistribution

The pressure–strain redistribution terms are the most important items in the closure because they control both the separation and the reattachment processes. The model used is an extension to rotating flows of the model developed by Gerolymos and Vallet.[97] The pressure–strain redistribution term augmented by the dissipation tensor anisotropy[107] is split into the slow and rapid parts and the corresponding echo terms. The slow part ϕ_{ij1} is modeled by a simple quasi-linear return-to-isotropy model whose coefficient has been optimized by Launder and Shima[107] to account for the anisotropic part of the dissipation tensor $\varepsilon_{ij} - \frac{2}{3}\delta_{ij}\varepsilon$. The closure for the rapid terms, which contains gradients of the mean velocity, must respect the Galilean invariance of ϕ_{ij2} (Ref. 108). Invariably the absolute flow mean velocity gradients are used.[109] For the quasi-linear isotropization-of-production model, this is equivalent to adding one-half of the Coriolis redistribution terms,[110] thus obtaining an isotropization-of-absolute-flow-production model.[111,112] The echo terms are computed in the usual way,[113] but the unit pseudonormal direction $\boldsymbol{e}_n = n_i \boldsymbol{e}_i$ is approximated by the gradient of a function of the turbulence lengthscale ℓ_T and of the Lumley flatness parameter[114] A, thus making the model independent of wall topology. The effect of the distance-from-the-wall is included in the functions C_1^w and C_2^w. The final model is

$$\phi_{ij} - \bar{\rho}\varepsilon_{ij} = \left[\phi_{ij} - \bar{\rho}\left(\varepsilon_{ij} - \frac{2}{3}\delta_{ij}\varepsilon\right)\right] - \frac{2}{3}\delta_{ij}\varepsilon$$

$$\cong \underbrace{-C_1\bar{\rho}\varepsilon a_{ij}}_{\phi_{ij1}} \underbrace{-C_2\left(P_{ij} + \frac{1}{2}G_{ij} - \frac{1}{3}\delta_{ij}P_{\ell\ell}\right)}_{\phi_{ij2}}$$

$$\underbrace{+C_1^w \frac{\varepsilon}{k}\left[\bar{\rho}\widetilde{w_k'' w_m''}n_k n_m \delta_{ij} - \frac{3}{2}\bar{\rho}\widetilde{w_k'' w_i''}n_k n_j - \frac{3}{2}\bar{\rho}\widetilde{w_k'' w_j''}n_k n_i\right]}_{\phi_{ij1}^w}$$

$$\underbrace{+C_2^w\left[\phi_{km2}n_k n_m \delta_{ij} - \frac{3}{2}\phi_{ik2}n_k n_j - \frac{3}{2}\phi_{jk2}n_k n_i\right]}_{\phi_{ij2}^w} - \frac{2}{3}\delta_{ij}\varepsilon \tag{15}$$

$$a_{ij} = \frac{\widetilde{w_i'' w_j''}}{k} - \frac{2}{3}\delta_{ij}, \qquad A_1 = a_{ii} = 0, \qquad A_2 = a_{ik}a_{ki}$$

$$A_3 = a_{ik}a_{kj}a_{ji}, \qquad A = \left[1 - \frac{9}{8}(A_2 - A_3)\right] \tag{16}$$

$$C_1 = 1 + 2.58A A_2^{\frac{1}{4}}\left\{1 - \exp\left[-\left(\frac{Re_T}{150}\right)^2\right]\right\}$$

$$C_2 = \min\left[1, 0.75 + 1.3\max\left[0, A - 0.55\right]\right]$$

$$\times A^{\left[\max(0.25, 0.5 - 1.3\max[0, A - 0.55])\right]}\left[1 - \max\left(0, 1 - \frac{Re_T}{50}\right)\right]$$

$$\boldsymbol{e}_n = n_i \boldsymbol{e}_i = \frac{\operatorname{grad}\ell_n}{\|\operatorname{grad}\ell_n\|}, \qquad \ell_n = \frac{\ell_T\{1 - \exp[-(Re_T/30)]\}}{1 + 2\sqrt{A_2} + 2A^{16}}$$

$$\ell_T = \frac{k^{\frac{3}{2}}}{\varepsilon}, \qquad C_1^w = 0.83\left[1 - \frac{2}{3}(C_1 - 1)\right]\left\|\operatorname{grad}\ell_1^w\right\|$$

$$\ell_1^w = \frac{\ell_T\{1 - \exp[-(Re_T/30)]\}}{1 + 2A_2^{0.8}}$$

$$C_2^w = \max\left[\frac{2}{3} - \frac{1}{6C_2}, 0\right]\left\|\operatorname{grad}\ell_2^w\right\|$$

$$\ell_2^w = \frac{\ell_T\{1 - \exp[-(Re_T/30)]\}}{1 + 1.8A_2^{\max(0.6, A)}} \tag{17}$$

Rotating Channel Flow

Fully developed incompressible plane channel flow subjected to spanwise rotation is an important test case where the Coriolis redistribution effect G_{ij} [Eq. (8)] has a major influence on the flow.[72] The flow is in the x-wise direction, and the rotation $\boldsymbol{\Omega} = \Omega \boldsymbol{e}_z$. The Coriolis effect on Reynolds stress redistribution diminishes turbulence levels on one side of the channel (stabilized side) and increases turbulence on the opposite side (destabilized side).[72,110,112] The simplified (fully developed two-dimensional) flow and turbulence model equations[72] are discretized using second-order accurate finite differences and are pseudotime-marched to machine-precision (15 digits) using a first-order accurate implicit procedure with approximate diagonalized Jacobians. Computational results for Reynolds numbers $Re_m = 1.15 \times 10^4$, and 3.5×10^4 ($Re_m = u_m D\nu^{-1}$, where

$$u_m = D^{-1}\int_0^D \bar{u}\,\mathrm{d}y$$

is the bulk velocity, D the channel height, and ν the kinematic viscosity) are compared with the measurements of Johnston et al.[72] The computational grid of N_j points used is stretched geometrically with ratio r_j, from centerline to the walls. For both Reynolds numbers, the nondimensional distance of the first node away from the wall $y_w^+ = \Delta y_w u_\tau \nu^{-1}$ is $\sim$0.25, and the grid size at the centerline is $\Delta y_{\mathrm{CL}} \cong 0.015D$ (Table 1).

The variation of friction velocity u_τ on the friction velocity at $\Omega = 0$ (u_{τ_0}), on the stabilized side ($y = D$ for $\Omega > 0$) and on the destabilized side ($y = 0$) as a function of the rotation (inverse Rosby) number $Ro_m^{-1} = \Omega D u_m^{-1}$ compares satisfactorily with experimental measurements (Fig. 1). For the lower Reynolds number ($Re_m = 1.15 \times 10^4$) the model starts relaminarizing at $Ro_m^{-1} \cong 0.07$ (in agreement with measurements[72]). However the predicted relaminarization is rather abrupt, giving a quasi-relaminarized stabilized side at $Ro_m^{-1} \cong 0.08$ (whereas measurements[72] indicate that the end of the relaminarization process takes place at $Ro_m^{-1} \cong 0.13$). This relaminarization behavior has been observed both experimentaly[72,115] and in low turbulence Reynolds number Re_T near-wall Reynolds stress computations.[112,116] Models using wall functions[110,117] cannot predict this behavior, which was also observed in direct numerical simulation computations.[118] Recently, Dutzler et al.[119] predicted correctly relaminarization in developing rotating plane channel flow, using a cubic ϕ_{ij2} closure consistant with the geostrophic constraint in the limit of rapidly rotating two-dimensional turbulence and elliptic near-wall relaxation. They observed, nonetheless, some discrepancies with measurements, which were partly attributed to three-dimensional effects in the experimental setup. It is possible that the fully developed flow constraint applied in the present computations adds to the difficulty of the problem.

Comparison of the velocity profiles at $Re_m = 3.5 \times 10^4$ for $Ro^{-1} = 0$, 0.042, and 0.068, shows satisfactory agreement between the present model predictions and measurements.[72] However, although the near-wall behavior is correct on both sides, the wake region of the destabilized side ($y < \frac{1}{2}D$) is not very well predicted. Such discrepancies were also observed by Dutzler et al.[119] and by Shima,[112] who attributed them to the unsatisfactory prediction of the "additive constant of the log-law in highly unstable wall regions, a typical difficulty in constructing models up to the wall." This is not surprising because for the relatively low Reynolds number flow considered, near-wall low turbulent Reynolds number Re_T modeling has a major influence on model predictions.[109] The observed

Table 1 Computational grids for rotating channel flow

$Re_m \times 10^4$	N_j	r_j	y_w^+ ($\Omega = 0$)	$\Delta y_{\mathrm{CL}} D^{-1}$
1.15	249	1.0294	0.265968	0.01464841
3.5	321	1.029	0.258054	0.01423838

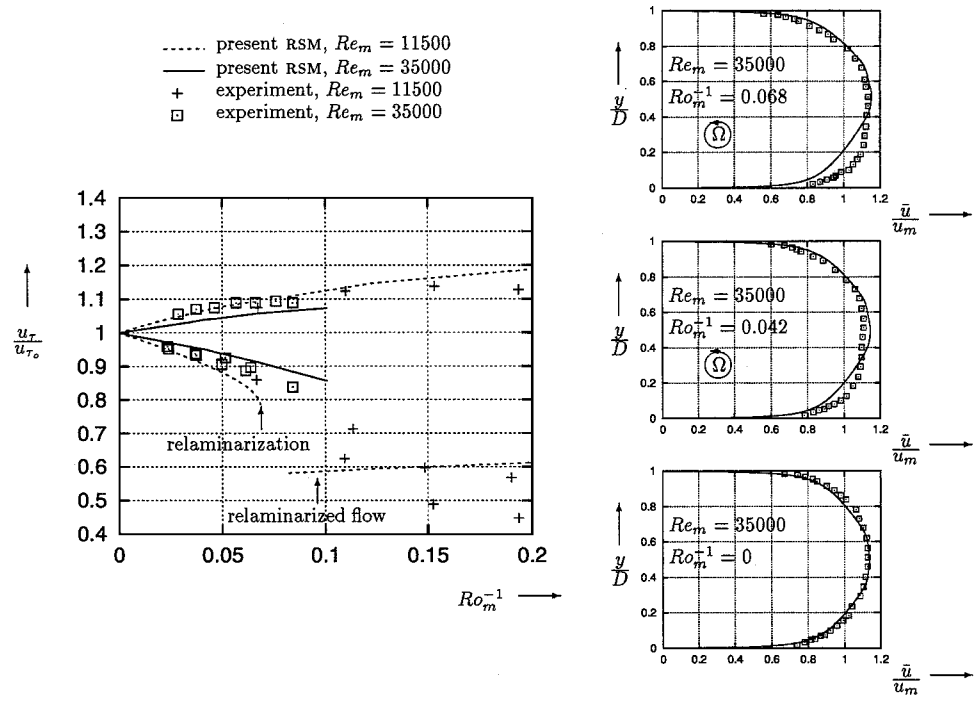

Fig. 1 Comparison of computed and measured[72] skin-friction and velocity distributions for fully developed rotating plane channel flow.

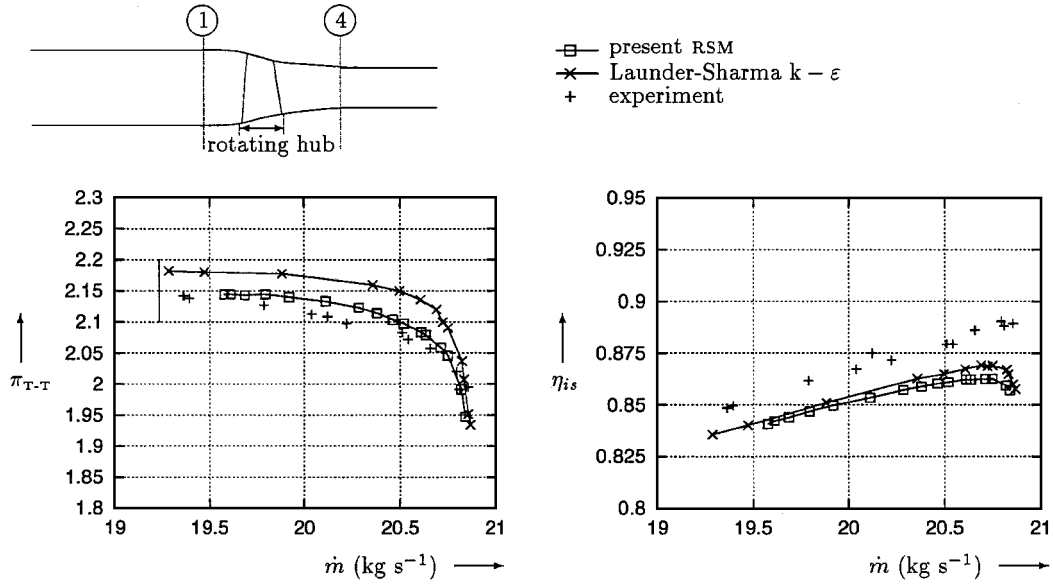

Fig. 2 Comparison of computed and measured[120] operating map of NASA 37 rotor.

discrepancies are partly attributed to the unsatisfactory transitional behavior of the ε equation used and are expected to be less important in high Reynolds number flows (the compressor test case studied in this paper is at $Re_\chi = W_{M_i}\chi\nu_i^{-1} \cong 10^6$, where W_{M_i} is the relative inflow velocity, ν_i is the kinematic viscosity at inflow conditions, and χ is the chord).

Transonic Compressor Rotor

Test Case

Computational results are compared with measurements for the NASA 37 transonic rotor.[22,99,120] In the (x, R, θ) coordinates system used, x is the engine axis ($\boldsymbol{\Omega} = \Omega\boldsymbol{e}_x$), R is the radius from the engine axis, and θ is the pitchwise coordinate ($\boldsymbol{e}_\theta = \boldsymbol{e}_x \times \boldsymbol{e}_R$). Experimental data for the NASA 37 transonic rotor were obtained at various measurement planes, using both laser Doppler velocimetry and classical rake measurements of pitchwise-averaged total pressure p_{t_M} and pitchwise-averaged total temperature T_{t_M}. [The averaging procedure $(\cdot)_M$ is described by Davis et al.[121]] This rotor has 36 blades, nominal speed 17188.7 rpm, and maximum mass flow at nominal speed $\dot{m}_{CH} = 20.93 \pm 0.14$ kg s^{-1} (Ref. 120). The measurement uncertainties reported by Suder[22] are mass flow $\pm 0.3\%$ kg $\cdot$ s^{-1}, flow angle ± 1 deg, total pressure ± 100 Pa, and total temperature ± 0.6 K. The nominal tip-clearance gap, which was used in the computations, is $\delta_{TC} = 0.356$ mm (Ref. 120).

This test case has been computed by numerous authors,[122] using either mixing-length[8,99] or two-equation closures.[47,49,50,53] The results thus obtained using various computational methods, tip-clearance flow simulations (embedded tip-clearance grid,[8,47,50,53] or simplified tip-clearance flow models[49,99]) and turbulence models show that the computations overestimate pressure ratio (at a given mass flow), over the entire span. Shabbir et al.[123] have shown that leakage flow emanating from a small gap between the stationary and rotating parts of the hub flowpath is responsible for a significant deficit of total pressure near the hub, but this cannot explain

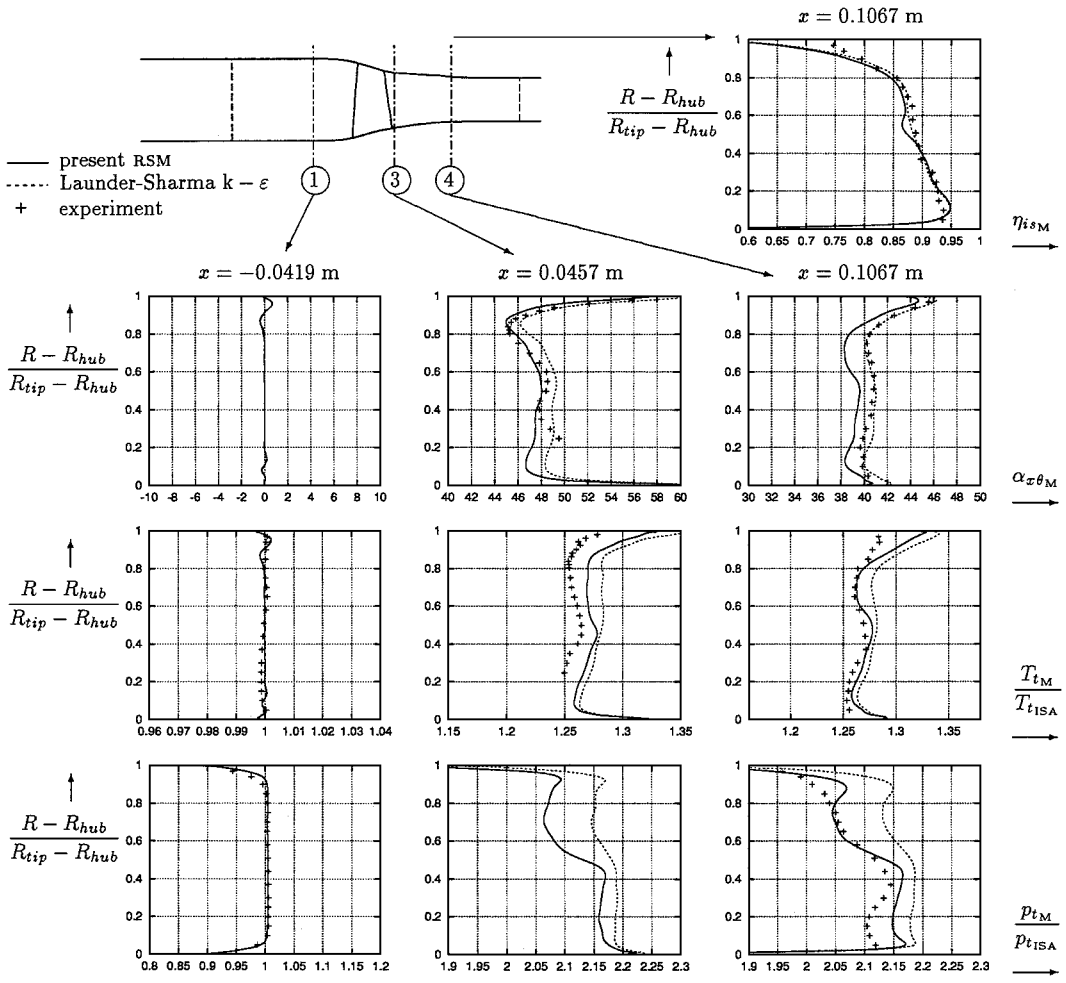

Fig. 3 Computed and measured radial distributions of pitchwise-averaged flow angle $\alpha_{x\theta_M}$, total pressure p_{t_M}, total temperature T_{t_M}, and isentropic efficiency η_{is_M}, for NASA 37 rotor ($\dot{m} = 20.51$ kg · s^{-1} = 0.98 $\dot{m}_{CH}$, $T_u = 3\%$, and $\delta_{TC} = 0.356$ mm).

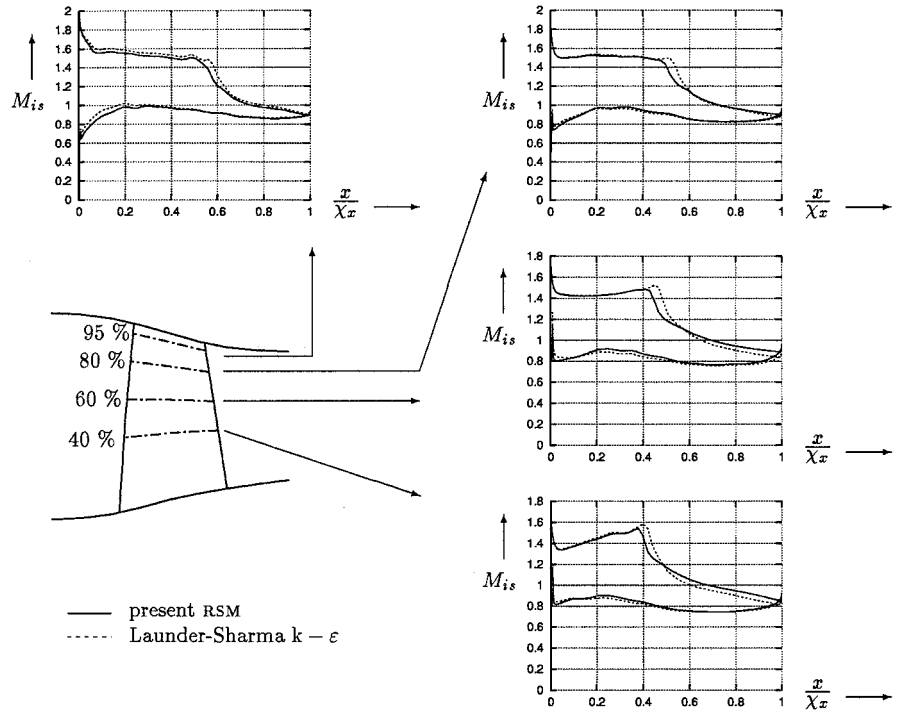

Fig. 4 Comparison of M_{is} distributions around the blades for NASA 37 rotor ($\dot{m} = 20.51$ kg · s^{-1} = 0.98 $\dot{m}_{CH}$, $T_u = 3\%$, and $\delta_{TC} = 0.356$ mm).

the observed discrepancies between measurement and computations farther away from the hub.

Computational Method

The grid used is generated biharmonically[124] and consists of five domains (Table 2): the upstream UH grid, the O grid around the blade, the downstream DH grid, the O grid of the tip-clearance gap (TC grid), and a buffer OZ grid between the TC grid and the O grid.[47] The grid topology used is described in detail by Gerolymos et al.[47] The total number of points is $\sim 3 \times 10^6$, with 161 radial stations (stretched near the hub and tip geometrically[124] with ratio $r_k = 1.17$). The nondimensional distance from the wall of the first grid point nearest to it $n_w^+ = \Delta n_w u_\tau \breve{\nu}_w^{-1}$ (where u_τ is the friction velocity, Δn_w the distance from the wall, and $\breve{\nu}_w$ the kinematic viscosity at the wall) is less than one-half everywhere. There are 41 radial stations within the tip-clearance gap (whose radial discretization is completely independent from the radial discretization of the blade O grid[47,124]). Grid convergence studies, comparing results on three different grids (1, 2, and 3×10^6 points), using the same numerical method but with k–ε closure,[57] have shown that this grid is sufficient to obtain grid-converged results.[47,53]

The mean-flow and turbulence-transport equations are written in the (x, y, z) Cartesian rotating (relative) coordinates system and are discretized in space, on a structured multiblock grid,

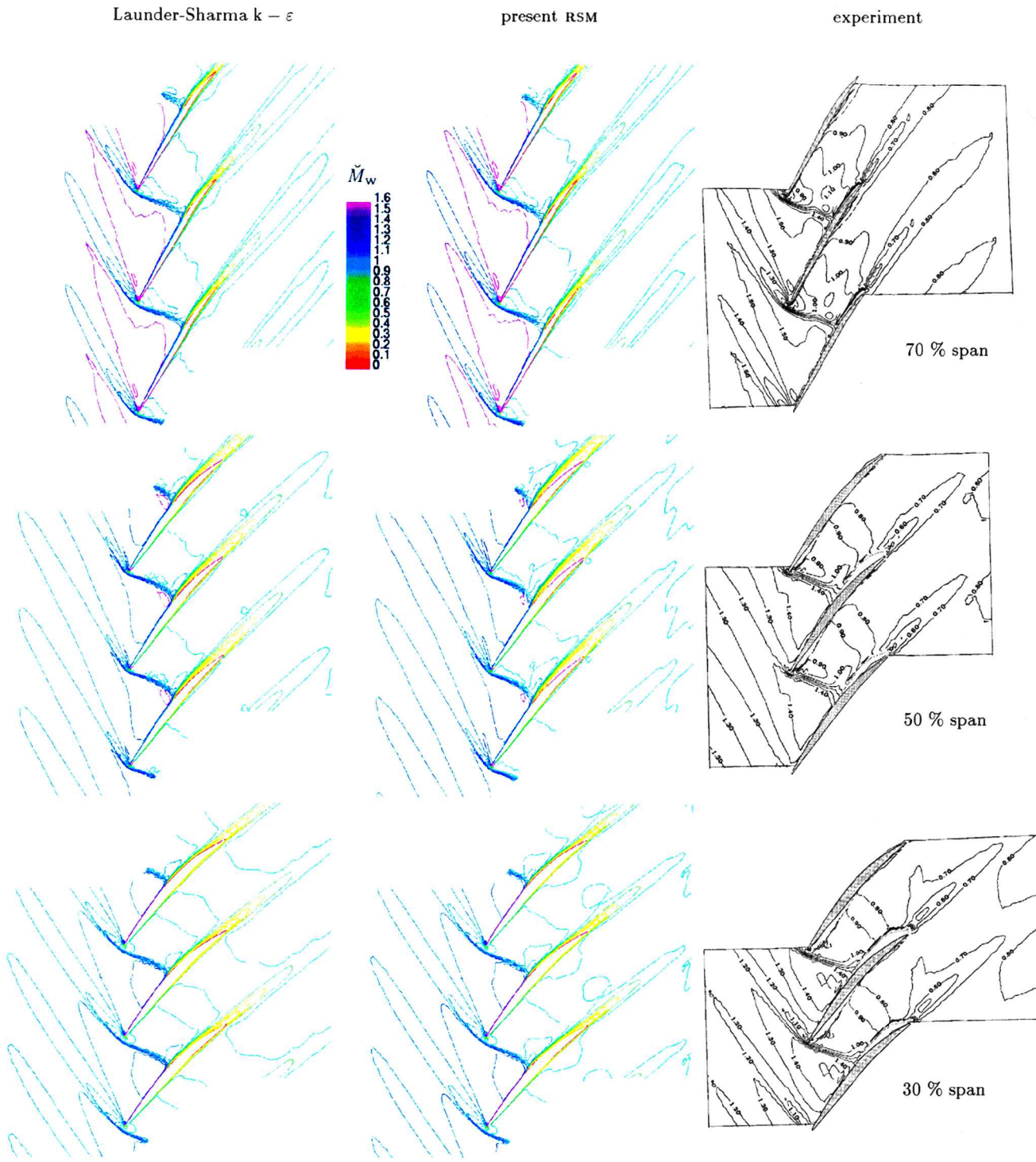

Fig. 5 Comparison of computed and measured $\breve{M}_w$ levels (step of 0.1 in the range $\breve{M}_w \in [0, 1.6]$ for both computations and measurements plotted at the same scale) for NASA 37 rotor ($\dot{m} = 20.51\ \mathrm{kg \cdot s^{-1}} = 0.98\ \dot{m}_{\mathrm{CH}}$, $T_u = 3\%$, and $\delta_{\mathrm{TC}} = 0.356$ mm).

Table 2 Computational grid summary[a]

Grid	Number
UH[b]	$49 \times 41 \times 161$
O[c]	$201 \times 53 \times 161$
DH[d]	$81 \times 61 \times 161$
TC[e]	$201 \times 17 \times 41$
OZ[f]	$201 \times 21 \times 61$
Points[g]	3,067,042
n_w^+	<0.5

[a]Grid topology is described in Gerolymos et al.[47]
[b]Upstream H grid (axial × tangential × radial).
[c]Blades O grid (around the blade × away from blade × radial).
[d]Downstream H grid (axial × tangential × radial).
[e]Tip-clearance O grid (around the blade × away from blade × radial).
[f]O zoom grid (around the blade × away from blade × radial).
[g]Without O-grid points overlapped by the OZ grid.

using a third-order upwind-biased MUSCL scheme with Van Leer flux-vector-splitting and Van Albada limiters, and the resulting semidiscrete scheme is integrated in time using a first-order implicit procedure (Refs. 47 and 101; Gerolymos and Vallet, manuscript in preparation). The mean-flow and turbulence-transportequations are integrated simultaneously. Source terms (centrifugal, Coriolis, and RSM) are treated explicitly because previous tests (Gerolymos and Vallet, manuscript in preparation) have shown that including the source Jacobians does not improve robustness. The local time step is based on a combined convective (Courant) and viscous (von Neumann) criterion. The boundary conditions, which are applied both explicitly and implicitly, using a phantom-nodes technique at grid interfaces, are described in detail by Gerolymos et al.[47] Inflow profiles of total pressure, total temperature and Reynolds stresses are obtained analytically in a manner similar to that of Gerolymos.[106] For the computations presented here, the inflow boundary-layer thicknesses at the hub and casing were $\delta_{\mathrm{HUB}_i} = \delta_{\mathrm{CSNG}_i} = 0.005$ m, and turbulence intensity outside of the boundary layers at inflow was $T_u = 3\%$, in accordance with experimental data.[120]

Comparison with Measurements

Comparison of computed and measured performance for the NASA 37 rotor (Fig. 2) indicates a substantial improvement in operating map (pressure ratio between stations 1 and 4 $\pi_{T\text{-}T}$ vs mass flow $\dot{m}$) prediction using the present RSM closure, compared to the Launder–Sharma k–ε model.[57] On the other hand, the prediction of efficiency is not improved (it is even marginally worse). A better understanding of the differences between the two turbulence closures is obtained through detailed comparisons at operating point A, corresponding to 98% of choke mass flow ($\dot{m} = 20.51\ \mathrm{kg \cdot s^{-1}} = 0.98\dot{m}_{\mathrm{CH}}$), where the values of $\pi_{T\text{-}T}$ are 1) experiment 2.075, 2) RSM 2.085 (error 0.5%), and 3) k–ε 2.145 (error 3.4%). The difference between the two models is substantial, especially if the results are considered in a multistage context, where the rotor is followed by a number of other blade rows. The overprediction by 3.4% of total pressure results in an overprediction by 3.4% of choke mass flow of the following blade row. As a consequence, if one of the following blade rows were designed with a very narrow choke margin, assuming a 3.4% higher than reality inlet total pressure may be sufficient to induce unstarted operating conditions, introducing multistage mismatch.[125] This is especially true if the same error is done on two or three blade rows because the errors have a cumulative effect.

Comparison of computed and measured pitchwise averaged quantities[121] (Fig. 3) shows that the present RSM closure improves the prediction of total-pressure p_{t_M}, from 40% span upward. The pressure deficit near the hub is of course not predicted, because hub leakage is not simulated. However, both models predict a p_{t_M} overshoot at the location of the tip-leakage vortex, attributed to unsatisfactory prediction of the mixing of the vortex with the main flow. Total temperature T_{t_M} is also better predicted by the new model, both near the rotor trailing edge (station 3) and farther downstream (station 4). The differences in flow angle $\alpha_{x\theta_M}$ between the two models and the experiment are within measurement accuracy.

To understand the mechanism of improvement of the results by the RSM closure, computed wall-pressure distributions around the blade (presented in terms of isentropic Mach number[32,35,106] M_{is}) around the blades are considered. For simplicity, the distributions are computed at constant span (and not along a meridional flow streamline). The reference total pressure at each span is taken, following the recommandation of Arnone,[126] equal to the maximum pressure on the blade at this span p_{SP}, whose location also defines the stagnation point on the blade (x_{SP}, R_{SP}). This pressure is corrected using rothalpy conservation at every point on the blade, and the isentropic Mach number is defined as

$$M_{\mathrm{is}} = \sqrt{\frac{2}{\gamma - 1}\left(\left(\frac{p_{\mathrm{SP}}}{p}\right)^{(\gamma-1)/\gamma}\left\{1 + \frac{\Omega^2\left(R^2 - R_{\mathrm{SP}}^2\right)}{2[\gamma/(\gamma-1)]R_g T_{\mathrm{SP}}}\right\} - 1\right)} \tag{18}$$

where T_{SP} is the stagnation-point temperature, and p and R are the local pressure and radius. Comparison of results obtained with the two turbulence models (experimental results of blade pressures are not available) shows that the RSM results predict the suction-side shock wave at ~5% axial chord (χ_x) farther upstream than the k–ε calculations (Fig. 4). The shock-wave/boundary-layer interaction is more important in the RSM results from 40% span upward, predicting lower pressure (higher M_{is}) downstream of the shock wave. The differences between the models are more difficult to discern on the relative Mach number $\breve{M}_W$ contours (Fig. 5), although the shock-wave/boundary-layer interaction predicted in the RSM computations is stronger (especially at 50% span), with a marked λ shock structure.

Conclusions

In the present work, a wall-normal-free, near-wall RSM was extended to flows with system rotation, in view of turbomachinery applications. The model gives satisfactory results when compared with experimental data for fully developed low-Reynolds-number turbulent channel flow subjected to spanwise rotation, although the prediction of the velocity profiles on the destabilized (more turbulent) side needs further improvement (presumably through modification of the baseline ε equation used). Nonetheless, the model gives the correct trends of the effects of rotation, while retaining a form completely independent of the distance-from-the-wall and of the normal-to-the-wall-direction, a definite advantage for complex geometry applications.

The model is then applied to the computation of three-dimensional transonic flow through a compressor rotor. The ability of the RSM closure to predict separation, improves three-dimensional blockage prediction. As a consequence, the computed compressor operating map is quite close to the experimental one, showing substantial improvement in comparison to k–ε computations. Both the total pressure and the total temperature rise are better predicted by the proposed RSM closure. The main remaining deficiency is the total pressure overshoot in the vicinity of the tip-clearance leakage vortex core location (also present in the k–ε results), presumably associated with the too slow relaxation behavior of the model (also observed in the process of boundary-layer reattachment after separation).

Although the proposed RSM closure can be further improved, the present results indicate that the use of advanced (anisotropic) turbulence closures enhances the quantitative prediction of the complex turbulent flows encountered in aircraft engine turbomachinery. The improvement is due both to a better prediction of separation and to the correct modeling of the Coriolis Reynolds stress redistribution effect (that is absent in Boussinesq-type closures such as mixing-length or k–ε).

Acknowledgments

The computations presented were run at the Institut pour le Développement des Ressources en Informatique Scientifique, where

computer resources were made available by the Comité Scientifique. Authors are listed alphabetically.

References

[1]Japikse, D., "Review—Progress in Numerical Turbomachinery Analysis," *Journal of Fluids Engineering*, Vol. 98, Dec. 1976, pp. 592–606.

[2]McNally, W. D., and Sockol, P. M., "Review—Computational Methods for Internal Flows with Emphasis on Turbomachinery," *Journal of Fluids Engineering*, Vol. 107, March 1985, pp. 6–22.

[3]Lakshminarayana, B., "An Assessment of Computational Fluid Dynamic Techniques in the Analysis and Design of Turbomachinery—The 1990 Freeman Scholar Lecture," *Journal of Fluids Engineering*, Vol. 113, Sept. 1991, pp. 315–352.

[4]Adamczyk, J. J., Celestina, M. L., Beach, T. A., and Barnett, M., "Simulation of 3-D Viscous Flow within a Multistage Turbine," *Journal of Turbomachinery*, Vol. 112, July 1990, pp. 370–376.

[5]Dawes, W. N., "Toward Improved Throughflow Capability: The Use of 3-D Viscous Flow Solvers in a Multistage Environment," *Journal of Turbomachinery*, Vol. 114, Jan. 1992, pp. 8–17.

[6]Denton, J. D., "The Calculation of 3-D Viscous Flow through Multistage Turbomachines," *Journal of Turbomachinery*, Vol. 114, Jan. 1992, pp. 18–26.

[7]Arnone, A., "Viscous Analysis of 3-D Rotor Flow using a Multigrid Method," *Journal of Turbomachinery*, Vol. 116, July 1994, pp. 435–445.

[8]Chima, R. V., "Calculation of Tip Clearance Effects in a Transonic Compressor Rotor," *Journal of Turbomachinery*, Vol. 120, Jan. 1998, pp. 131–140.

[9]Rhie, C. M., Gleixner, A. J., Spear, D. A., Fischberg, C. J., and Zacharias, R. M., "Development and Application of a Multistage Navier–Stokes Solver: Part I—Multistage Modeling using Bodyforces and Deterministic Stresses," *Journal of Turbomachinery*, Vol. 120, April 1998, pp. 205–214.

[10]LeJambre, C. R., Zacharias, R. M., Biederman, B. P., Gleixner, A. J., and Yetka, C. J., "Development and Application of a Multistage Navier–Stokes Solver: Part II—Application to a High-Pressure Compressor Design," *Journal of Turbomachinery*, Vol. 120, April 1998, pp. 215–223.

[11]Gallus, H. E., Hah, C., and Schulz, H. D., "Experimental and Numerical Investigation of 3-D Viscous Flows and Vortex Motion Inside an Annular Compressor Blade-Row," *Journal of Turbomachinery*, Vol. 113, April 1991, pp. 198–206.

[12]Adamczyk, J. J., Celestina, M. L., and Chen, J. P., "Wake-Induced Unsteady Flows: Their Impact on Rotor Performance and Wake Rectification," *Journal of Turbomachinery*, Vol. 118, Jan. 1996, pp. 88–95.

[13]Turner, M. G., "Multiblade Turbine Simulations with Vortex-Blade Interaction," *Journal of Turbomachinery*, Vol. 118, Oct. 1996, pp. 643–653.

[14]Jennions, I. K., and Adamczyk, J. J., "Evaluation of the Interaction Losses in a Transonic Turbine HP-Rotor/LP-Vane Configuration," *Journal of Turbomachinery*, Vol. 119, Jan. 1997, pp. 68–76.

[15]Hah, C., Puterbaugh, S. L., and Copenhaver, W. W., "Unsteady Aerodynamic Flow Phenomena in a Transonic Compressor Stage," *Journal of Propulsion and Power*, Vol. 13, No. 3, 1997, pp. 329–333.

[16]Hah, C., Rabe, D. C., Sullivan, T. J., and Wadia, A. R., "Effects of Inlet Distortion on the Flow Field in a Transonic Compressor Rotor," *Journal of Turbomachinery*, Vol. 120, April 1998, pp. 233–246.

[17]Volmar, T. W., Brouillet, B., Gallus, H. E., Benetschik, H., "Time-Accurate Three-Dimensional Navier–Stokes Analysis of $1\frac{1}{2}$-Stage Axial-Flow Turbine," *Journal of Propulsion and Power*, Vol. 16, No. 2, 2000, pp. 327–335.

[18]Sieverding, C. H., "Recent Progress in the Understanding of Basic Aspects of Secondary Flows in Turbine Blade Passages," *Journal of Engineering for Gas Turbines and Power*, Vol. 107, April 1985, pp. 248–257.

[19]Leylek, J. H., and Wisler, D. C., "Mixing in Axial-Flow Compressors: Conclusions Drawn from 3-D Navier–Stokes Analyses and Experiments," *Journal of Turbomachinery*, Vol. 113, April 1991, pp. 139–160.

[20]Adamczyk, J. J., Celestina, M. L., and Greitzer, E. M., "The Role of Tip Clearance in High-Speed Fan Stall," *Journal of Turbomachinery*, Vol. 115, Jan. 1993, pp. 28–39.

[21]Denton, J. D., "Loss Mechanisms in Turbomachines," *Journal of Turbomachinery*, Vol. 115, Oct. 1993, pp. 621–656.

[22]Suder, K. L., "Blockage Development in a Transonic Axial Compressor Rotor," *Journal of Turbomachinery*, Vol. 120, July 1998, pp. 465–476.

[23]Furukawa, M., Inoue, M., Saiki, K., Yamada, K., "The Role of Tip Leakage Vortex Breakdown in Compressor Rotor Aerodynamics," *Journal of Turbomachinery*, Vol. 121, July 1999, pp. 469–480.

[24]Baskharone, E. A., and Wyman, N. J., "Primary/Leakage Flow Interaction in a Pump Stage," *Journal of Fluids Engineering*, Vol. 121, March 1999, pp. 133–138.

[25]Wellborn, S. R., and Okiishi, T. H., "The Influence of Shrouded Cavity Flows on Multistage Compressor Performance," *Journal of Turbomachinery*, Vol. 121, July 1999, pp. 486–498.

[26]Wellborn, S. R., Tolchinsky, I., and Okiishi, T. H., "Modeling Shrouded Stator Cavity Flows in Axial-Flow Compressors," *Journal of Turbomachinery*, Vol. 122 , Jan. 2000, pp. 55–61.

[27]Kaszeta, R. W., and Simon, T. W., "Measurement of Eddy Diffusivity of Momentum in Film Cooling Flows with Streamwise Injection," *Journal of Turbomachinery*, Vol. 122, Jan. 2000, pp. 178–183.

[28]Bohn, D., Becker, V., Kusterer, K., Fottner, L., and Ardey, S., "Three-Dimensional Flow Analysis of Turbine Blade Cascades with Leading-Edge Ejection," *Journal of Propulsion and Power*, Vol. 16, No. 1, 2000, pp. 49–56.

[29]Lakshminarayana, B., "Turbulence Modeling for Complex Shear Flows," *AIAA Journal*, Vol. 24, No. 12, 1986, pp. 1900–1917.

[30]Launder, B. E., "2-Moment Closure: Present . . . and Future?," *International Journal of Heat and Fluid Flow*, Vol. 10, No. 4, 1989, pp. 282–300.

[31]Hanjalić, K., "Advanced Turbulence Closure Models: A View of Current Status and Future Prospects," *International Journal of Heat and Fluid Flow*, Vol. 15, No. 3, 1994, pp. 178–203.

[32]Leschziner, M. A., "Computation of Aerodynamic Flows with Turbulence-Transport Models Based on 2-Moment Closure," *Computers and Fluids*, Vol. 24, No. 4, 1995, pp. 377–392.

[33]Bradshaw, P., "Turbulence Modeling with Application to Turbomachinery," *Progress in Aerospace Sciences*, Vol. 32, 1996, pp. 575–624.

[34]Hah, C., "A Numerical Modeling of Endwall and Tip-Clearance Flow of an Isolated Compressor Rotor," *Journal of Engineering for Gas Turbines and Power*, Vol. 108, Jan. 1986, pp. 15–21.

[35]Hah, C., "Calculation of Three-Dimensional Viscous Flows in Turbomachinery with an Implicit Relaxation Method," *Journal of Propulsion and Power*, Vol. 3, No. 5, 1987, pp. 415–422.

[36]Hah, C., Bryans, A. C., Moussa, Z., and Tomsho, M. E., "Application of Viscous Flow Computations for the Aerodynamic Performance of a Backswept Impeller at Various Operating Conditions," *Journal of Turbomachinery*, Vol. 110, July 1988, pp. 303–311.

[37]Hah, C., and Krain, H., "Secondary Flows and Vortex Motion in a High-Efficiency Backswept Impeller at Design and Off-Design Conditions," *Journal of Turbomachinery*, Vol. 112, Jan. 1990, pp. 7–13.

[38]Hah, C., and Wennerstrom, A. J., "3-D Flowfields inside a Transonic Compressor with Swept Blades," *Journal of Turbomachinery*, Vol. 113, April 1991, pp. 241–251.

[39]Hah, C., and Reid, L., "A Viscous Flow Study of Shock/Boundary-Layer Interaction, Radial Transport, and Wake Development in a Transonic Compressor," *Journal of Turbomachinery*, Vol. 114, July 1992, pp. 538–547.

[40]Kunz, R. F., and Lakshminarayana, B., "3-D Navier–Stokes Computation of Turbomachinery Flows using an Explicit Numerical Procedure and a Coupled k–ε Turbulence Model," *Journal of Turbomachinery*, Vol. 114, July 1992, pp. 627–642.

[41]Copenhaver, W. W., Hah, C., and Puterbaugh, S. L., "3-D Flow Phenomena in a Transonic, High-Throughflow, Axial-Flow Compressor Stage," *Journal of Turbomachinery*, Vol. 115, April 1993, pp. 240–248.

[42]Copenhaver, W. W., Mayhew, E. R., Hah, C., and Wadia, A. R., "The Effect of Tip Clearance on a Swept Transonic Compressor Rotor," *Journal of Turbomachinery*, Vol. 118, April 1996, pp. 230–239.

[43]Copenhaver, W. W., Puterbaugh, S. L., and Hah, C., "Unsteady Flow and Shock Motion in a Transonic Compressor Rotor," *Journal of Propulsion and Power*, Vol. 13, No. 1, 1997, pp. 17–23.

[44]Puterbaugh, S. L., and Brendel, M., "Tip-Clearance-Flow/Shock Interaction in a Transonic Compressor Rotor," *Journal of Propulsion and Power*, Vol. 13, No. 1, 1997, pp. 24–30.

[45]Koiro, M., and Lakshminarayana, B., "Simulation and Validation of Mach-Number Effects on Secondary Flow in a Transonic Turbine Cascade using a Multigrid k–ε Solver," *Journal of Turbomachinery*, Vol. 120, April 1998, pp. 285–297.

[46]Ameri, A. A., Steinthorsson, E., and Rigby, D. L., "Effect of Squealer Tip on Rotor Heat Tranfer and Efficiency," *Journal of Turbomachinery*, Vol. 120, Oct. 1998, pp. 753–759.

[47]Gerolymos, G. A., Tsanga, G., and Vallet, I., "Near-Wall k–ε Computation of Transonic Turbomachinery Flows with Tip Clearance," *AIAA Journal*, Vol. 36, No. 10, 1998, pp. 1769–1777.

[48]Gerolymos, G. A., and Hanisch, C., "Multistage 3-D Navier–Stokes Computation of Off-Design Operation of a 4-Stage Turbine," *Journal of Power and Energy*, Vol. 213, 1999, pp. 243–261.

[49]Arima, T., Sonoda, T., Shirotori, M., Tamura, A., and Kikuchi, K., "A Numerical Investigation of Transonic Axial Compressor Rotor Flow Using a Low-Reynolds-Number k–ε Turbulence Model," *Journal of Turbomachinery*, Vol. 121, Jan. 1999, pp. 44–58.

[50]Hah, C., and Loellbach, J., "Development of Hub Corner Stall and Its Influence on the Performance of Axial Compressor Blade Rows," *Journal of Turbomachinery*, Vol. 121, Jan. 1999, pp. 67–77.

[51]Ameri, A. A., Steinthorsson, E., and Rigby, D. L., "Effects of Tip-Clearance and Casing Recess on Heat Transfer and Stage Efficiency in Axial Turbines," *Journal of Turbomachinery*, Vol. 121, Oct. 1999, pp. 683–693.

[52]Hildebrandt, T., and Fottner, L., "A Numerical Study of the Influence of Grid Refinement and Turbulence Modeling on the Flow Field Inside a Highly Loaded Turbine Cascade," *Journal of Turbomachinery*, Vol. 121, Oct. 1999, pp. 709–716.

[53]Gerolymos, G. A., and Vallet, I., "Tip-Clearance and Secondary Flows in a Transonic Compressor Rotor," *Journal of Turbomachinery*, Vol. 121, Oct. 1999, pp. 751–762.

[54]Chernobrovkin, A., and Lakshminarayana, B., "Turbulence Modeling and Computation of Viscous Transitional Flow for Low Pressure Turbines," *Journal of Fluids Engineering*, Vol. 121, Dec. 1999, pp. 824–833.

[55]Jones, W. P., and Launder, B. E., "The Prediction of Laminarization with a 2-Equation Model of Turbulence," *International Journal of Heat and Mass Transfer*, Vol. 15, 1972, pp. 301–314.

[56]Jones, W. P., and Launder, B. E., "The Calculation of Low-Reynolds-Number Phenomena with a 2-Equation Model of Turbulence," *International Journal of Heat and Mass Transfer*, Vol. 16, 1973, pp. 1119–1130.

[57]Launder, B. E., and Sharma, B. I., "Application of the Energy Dissipation Model of Turbulence to the Calculation of Flows near a Spinning Disk," *Letters in Heat and Mass Transfer*, Vol. 1, 1974, pp. 131–138.

[58]Wilcox, D. C., "Simulation of Transition with a 2-Equation Turbulence Model," *AIAA Journal*, Vol. 32, No. 2, 1994, pp. 247–255.

[59]Wilcox, D. C., "Reassessment of the Scale-Determining Equation for Advanced Turbulence Models," *AIAA Journal*, Vol. 26, No. 11, 1988, pp. 1299–1310.

[60]Speziale, C. G., "On Nonlinear k–ℓ and k–ε Models of Turbulence," *Journal of Fluid Mechanics*, Vol. 178, 1987, pp. 459–475.

[61]Speziale, C. G., Abid, R., and Anderson, E. C., "Critical Evaluation of 2-Equation Models for Near-Wall Turbulence," *AIAA Journal*, Vol. 30, No. 2, 1992, pp. 324–331.

[62]Robinson, D. F., and Hassan, H. A., "Further Development of the k–ζ (Enstrophy) Turbulence Closure Model," *AIAA Journal*, Vol. 36, No. 10, 1998, pp. 1825–1833.

[63]Stock, H. W., and Haase, W., "Determination of Length Scales in Algebraic Turbulence Models for Navier–Stokes Methods," *AIAA Journal*, Vol. 27, No. 1, 1989, pp. 5–14.

[64]Mavriplis, D. J., "Algebraic Turbulence Modeling for Unstructured and Adaptive Meshes," *AIAA Journal*, Vol. 29, No. 12, 1991, pp. 2086–2093.

[65]Ekaterinaris, J. A., and Menter, F. R., "Computation of Oscillating Airfoil Flows with One- and Two-Equation Turbulence Models," *AIAA Journal*, Vol. 32, No. 12, 1994, pp. 2359–2365.

[66]Patel, V. G., Rodi, W., and Scheuerer, G., "Turbulence Models for Near-Wall and Low Reynolds Number Flows: A Review," *AIAA Journal*, Vol. 23, No. 9, 1985, pp. 1308–1319.

[67]Menter, F. R., "Performance of Popular Turbulence Models for Attached and Separated Adverse-Pressure-Gradient Flows," *AIAA Journal*, Vol. 30, No. 8, 1992, pp. 2066–2072.

[68]Wilcox, D. C., "Comparison of Two-Equation Turbulence Models for Boundary-Layers with Pressure-Gradient," *AIAA Journal*, Vol. 31, No. 8, 1993, pp. 1414–1421.

[69]Menter, F. R., "Two-Equation Eddy-Viscosity Turbulence Models for Engineering Applications," *AIAA Journal*, Vol. 32, No. 8, 1994, pp. 1598–1605.

[70]Goldberg, U., Peroomian, O., and Chakravarthy, S., "A Wall-Distance-Free k–ε Model with Enhanced Near-Wall Treatment," *Journal of Fluids Engineering*, Vol. 120, Sept. 1998, pp. 457–462.

[71]Bradshaw, P., "The Analogy between Streamline Curvature and Buoyancy in Turbulent Shear Flow," *Journal of Fluid Mechanics*, Vol. 36, 1969, pp. 177–191.

[72]Johnston, J. P., Halleen, R. M., and Lezius, D. K., "Effects of Spanwise Rotation on the Structure of 2-D Fully Developed Turbulent Channel Flow," *Journal of Fluid Mechanics*, Vol. 56, 1972, pp. 533–557.

[73]Launder, B. E., Reece, G. J., and Rodi, W., "Progress in the Development of a Reynolds-Stress Turbulence Closure," *Journal of Fluid Mechanics*, Vol. 68, 1975, pp. 537–566.

[74]Launder, B. E., "A Generalized Algebraic Stress Transport Hypothesis," *AIAA Journal*, Vol. 20, No. 3, 1982, pp. 436–437.

[75]Gatski, T. B., and Speziale, C. G., "On Explicit Algebraic Stress Models for Complex Turbulent Flows," *Journal of Fluid Mechanics*, Vol. 254, 1993, pp. 59–78.

[76]Schiestel, R., "Multiple-Time-Scales Modeling of Turbulent Flows in One-Point Closures," *Physics of Fluids*, Vol. 30, No. 3, 1987, pp. 722–731.

[77]Wilcox, D. C., "Multiscale Model for Turbulent Flows," *AIAA Journal*, Vol. 26, No. 11, 1988, pp. 1311–1320.

[78]Kim, S. W., "Numerical Investigation of Separated Transonic Turbulent Flows with a Multiple-Time-Scale Turbulence Model," *Numerical Heat Transfer A*, Vol. 18, 1990, pp. 149–171.

[79]Liou, W. W., Shih, T. H., and Duncan, B. S., "A Multiple-Scale Model for Compressible Turbulent Flows," *Physics of Fluids*, Vol. 7, No. 3, 1995, pp. 658–666.

[80]Gleize, V., Schiestel, R., and Couailler, V., "Multiple-Scale Modeling of Turbulent Nonequilibrium Boundary-Layer Flows," *Physics of Fluids*, Vol. 8, No. 10, 1996, pp. 2716–2732.

[81]Grégoire, O., Souffland, D., Gauthier, S., and Schiestel, R., "A 2-Time-Scale Turbulence Model for Compressible Flows: Turbulence Dominated by Mean Deformation Interaction," *Physics of Fluids*, Vol. 11, No. 12, 1999, pp. 3793–3807.

[82]Craft, T. J., Launder, B. E., and Suga, K., "Development and Application of a Cubic Eddy-Viscosity Model of Turbulence," *International Journal of Heat and Fluid Flow*, Vol. 17, 1996, pp. 108–115.

[83]Craft, T. J., Launder, B. E., and Suga, K., "Prediction of Turbulent Transitional Phenomena with a Nonlinear Eddy-Viscosity Model," *International Journal of Heat and Fluid Flow*, Vol. 18, 1997, pp. 15–28.

[84]Speziale, C. G., "Comparison of Explicit and Traditional Algebraic Stress Models of Turbulence," *AIAA Journal*, Vol. 35, No. 9, 1997, pp. 1506–1509.

[85]Carlson, J. R., "Applications of Algebraic Reynolds Stress Turbulence Models, Part 1: Incompressible Flat Plate," *Journal of Propulsion and Power*, Vol. 13, No. 5, 1997, pp. 610–619.

[86]Carlson, J. R., "Applications of Algebraic Reynolds Stress Turbulence Models, Part 2: Transonic Shock-Separated Afterbody," *Journal of Propulsion and Power*, Vol. 13, No. 5, 1997, pp. 620–628.

[87]Rizzetta, D. P., "Evaluation of Explicit Algebraic Reynolds-Stress Models for Separated Supersonic Flows," *AIAA Journal*, Vol. 36, No. 1, 1998, pp. 24–30.

[88]Sotiropoulos, F., and Ventikos, Y., "Flow Through a Curved Duct Using Nonlinear Two-Equation Turbulence Models," *AIAA Journal*, Vol. 36, No. 7, 1998, pp. 1256–1262.

[89]Barakos, G., and Drikakis, D., "Investigation of Nonlinear Eddy-Viscosity Turbulence Models in Shock/Boundary-Layer Interaction," *AIAA Journal*, Vol. 38, No. 3, 2000, pp. 461–469.

[90]Sotiropoulos, F., and Patel, V. C., "Prediction of Turbulent Flow Through a Transition Duct Using a Two-Moment Closure," *AIAA Journal*, Vol. 32, No. 11, 1994, pp. 2194–2204.

[91]Sotiropoulos, F., and Patel, V. C., "Application of Reynolds-Stress Transport Models to Stern and Wake Flows," *Journal of Ship Research*, Vol. 39, No. 4, 1995, pp. 263–283.

[92]Ladeinde, F., "Supersonic Flux-Split Procedure for Two-Moments of Turbulence," *AIAA Journal*, Vol. 33, No. 7, 1995, pp. 1185–1195.

[93]Gerolymos, G. A., and Vallet, I., "Near-Wall Reynolds-Stress Three-Dimensional Transonic Flows Computation," *AIAA Journal*, Vol. 35, No. 2, 1997, pp. 228–236.

[94]Chenault, C. F., and Beran, P. S., "k–ε and Reynolds Stress Turbulence Model Comparisons for Two-Dimensional Injection Flows," *AIAA Journal*, Vol. 36, No. 8, 1998, pp. 1401–1412.

[95]Chenault, C. F., Beran, P. S., and Bowersox, R. D. W., "Numerical Investigation of Supersonic Injection using a Reynolds-Stress Turbulence Model," *AIAA Journal*, Vol. 37, No. 10, 1999, pp. 1257–1269.

[96]Batten, P., Craft, T. J., Leschziner, M. A., and Loyau, H., "Reynolds-Stress-Transport Modeling for Compressible Aerodynamics Applications," *AIAA Journal*, Vol. 37, No. 7, 1999, pp. 785–797.

[97]Gerolymos, G. A., and Vallet, I., "Wall-Normal-Free Reynolds-Stress Closure for Three-Dimensional Compressible Separated Flows," *AIAA Journal*, Vol. 39, No. 10, 2001, pp. 1833–1842.

[98]Schumann, U., "Realizability of Reynolds-Stress Turbulence Models," *Physics of Fluids*, Vol. 20, No. 5, 1977, pp. 721–725.

[99]Suder, K. L., and Celestina, M. L., "Experimental and Computational Investigation of the Tip-Clearance Flow in a Transonic Axial Compressor Rotor," *Journal of Turbomachinery*, Vol. 118, April 1996, pp. 218–229.

[100]Aris, R., *Vectors, Tensors, and the Basic Equations of Fluid Mechanics*, Dover, New York, 1962, pp. 10, 16.

[101]Gerolymos, G. A., and Vallet, I., "Implicit Computation of the Three-Dimensional Compressible Navier–Stokes Equations Using k–ε Turbulence Closure," *AIAA Journal*, Vol. 34, No. 7, 1996, pp. 1321–1330.

[102]Smits, A. J., and Dussauge, J. P., *Turbulent Shear Layers in Supersonic Flow*, AIP Press, Woodbury, NY, 1996, p. 78.

[103]Vandromme, D., and Ha Minh, H., "About the Coupling of Turbulence Closure Models with Averaged Navier–Stokes Equations," *Journal of Computational Physics*, Vol. 65, 1986, pp. 386–409.

[104]Sarkar, S., Erlebacher, G., Hussaini, M. Y., and Kreiss, H. O., "The Analysis and Modelling of Dilatational Terms in Compressible Turbulence," *Journal of Fluid Mechanics*, Vol. 227, 1991, pp. 473–493.

[105]Hanjalić, K., and Launder, B. E., "A Reynolds Stress Model of Turbulence and Its Application to Thin Shear Flows," *Journal of Fluid Mechanics*, Vol. 52, 1972, pp. 609–638.

[106]Gerolymos, G. A., "Implicit Multiple-Grid Solution of the Compressible Navier–Stokes Equations Using k–ε Turbulence Closure," *AIAA Journal*, Vol. 28, No. 10, 1990, pp. 1707–1717.

[107]Launder, B. E., and Shima, N., "Two-Moment Closure for the Near-Wall Sublayer: Development and Application," *AIAA Journal*, Vol. 27, No. 10, 1989, pp. 1319–1325.

[108]Speziale, C. G., "Turbulence Modeling in Noninertial Frames of Reference," *Theoretical and Computational Fluid Dynamics*, Vol. 1, 1989, pp. 3–19.

[109] Speziale, C. G., Younis, B. A., and Berger, S. A., "Analysis and Modelling of Turbulent Flow in an Axially Rotating Pipe," *Journal of Fluid Mechanics*, Vol. 407, 2000, pp. 1–26.

[110] Launder, B. E., Tselepidakis, D. P., and Younis, B. A., "A Second-Moment Closure Study of Rotating Channel Flow," *Journal of Fluid Mechanics*, Vol. 183, 1987, pp. 63–75.

[111] Shima, N., "Prediction of Turbulent Boundary-Layer Flows with a 2-Moment Closure: Part I—Effects of Periodic Pressure Gradient, Wall Transpiration, and Free-Stream Turbulence," *Journal of Fluids Engineering*, Vol. 115, March 1993, pp. 56–63.

[112] Shima, N., "Prediction of Turbulent Boundary-Layer Flows with a 2-Moment Closure: Part II—Effects of Streamline Curvature and Spanwise Rotation," *Journal of Fluids Engineering*, Vol. 115, March 1993, pp. 64–69.

[113] Gibson, M. M., and Launder, B. E., "Ground Effects on Pressure Fluctuations in the Atmospheric Boundary Layer," *Journal of Fluid Mechanics*, Vol. 86, 1978, pp. 491–511.

[114] Lumley, J. L., "Computational Modeling of Turbulent Flows," *Advances in Applied Mechanics*, Vol. 18, 1978, pp. 123–176.

[115] Nakabayashi, K., and Kitoh, O., "Low-Reynolds-Nimber Fully Developed 2-D Turbulent Channel Flow with System Rotation," *Journal of Fluid Mechanics*, Vol. 315, 1996, pp. 1–29.

[116] Launder, B. E., and Tselepidakis, D. P., "Application of a New Second-Moment Closure to Turbulent Channel Flow Rotating in Orthogonal Mode," *International Journal of Heat and Fluid Flow*, Vol. 15, No. 1, 1994, pp. 2–10.

[117] Younis, B. A., Speziale, C. G., and Berger, S. A., "Accounting for Effects of a System Rotation on the Pressure–Strain Correlation," *AIAA Journal*, Vol. 36, No. 9, 1998, pp. 1746–1748.

[118] Kristoffersen, R., and Andersson, H. I., "Direct Simulations of Low-Reynolds-Number Turbulent Flow in a Rotating Channel," *Journal of Fluid Mechanics*, Vol. 256, 1993, pp. 163–197.

[119] Dutzler, G. K., Pettersson-Reif, B. A., and Andersson, H. I., "Relaminarization of Turbulent Flow in the Entrance Region of Rapidly Rotating Channel," *International Journal of Heat and Fluid Flow*, Vol. 21, 2000, pp. 49–57.

[120] Strazisar, A. J., "Data Report and Data Diskette for NASA Transonic Compressor Rotor 37," NASA Lewis Research Center, 1994.

[121] Davis, R. L., Delaney, R. A., Denton, J. D., Giles, M. B., Strazisar, A. J., and Wisler, D. C., "CFD Code Assessment in Turbomachinery—Author's Information Package," American Society of Mechanical Engineers Turbomachinery Committee, 1993.

[122] Denton, J. D., "Lessons Learned from Rotor 37," Third International Symposium on Experimental and Computational Aerothermodynamics of Internal Flows (ISAIF), Sept. 1996.

[123] Shabbir, A., Celestina, M. L., Adamczyk, J. J., and Strazisar, A. J., "The Effect of Hub Leakage on 2 High Speed Axial Flow Compressor Rotors," American Society of Mechanical Engineers, ASME Paper 97-GT-346, 1997.

[124] Gerolymos, G. A., and Tsanga, G., "Biharmonic Three-Dimensional Grid Generation for Axial Turbomachinery with Tip Clearance," *Journal of Propulsion and Power*, Vol. 15, No. 3, 1999, pp. 476–479.

[125] Cumpsty, N. A., *Compressor Aerodynamics*, Longman, 1989, p. 83.

[126] Arnone, A., Project APPACET Meeting, Turin, Italy, 1999.

R. M. C. So
Associate Editor

Color reproduction courtesy of Université Pierre-et-Marie-Curie.